Fast near-region gravity terrain correction approach based on panoramic stereo vision

DI Kaichang[1]   WU Kai[1]   LIU Zhaoqin[1]   WAN Wenhui[1]   DI Zhizhong[2]   LI Gang[2]

1. *State Key Laboratory of Remote Sensing Science   Jointly Sponsored by the Institute of Remote Sensing and Digital Earth   Chinese Academy of Sciences and Beijing Normal University   Beijing 100101   China;*
2. *Beijing Explo-Tech Engineering Co.   Ltd.   Beijing 100085   China*

Abstract: Gravity terrain correction is a critical step in regional gravity survey. The main challenge for gravity terrain correction is how to rapidly and inexpensively reconstruct high-quality terrain near the gravity survey station. This paper proposes a fast near-region terrain correction approach based on panoramic stereo vision and photogrammetry techniques. A fast and low-cost topographic mapping system is designed and developed for this purpose. To miniaturize the system and assure required mapping accuracy   we theoretically analyze and optimize the hardware design. The developed software system generates DEM automatically from panoramic stereo images and calculates the gravity correction value at each station. The system has been verified in several filed tests with various terrain circumstances. The test results demonstrate that the developed gravity terrain correction method s ignificantly outperforms the traditional field surveying methods in efficiency and accuracy.

Key words: gravity terrain correction   topographic mapping   panoramic vision   stereo image matching   point cloud filtering

1   INTRODUCTION

Gravity terrain correction is an important procedure for o btaining Bouguer gravity anomaly during regional gravity sur-vey (Yen et al.   1994). Terrain correction is normally cat-egorized into three parts by the range from the gravity station   one part being correction for terrain relatively close to the sur-vey s tation as far as 20—50 m   commonly known as near re-gion t errain correction (Fan   2007)   while the other two parts for more distant terrain   referred as mid region terrain correction and far region terrain correction. Currently   for the mid and far region parts   computer aided programs have been introduced to automate the terrain correction procedure based on widely available topographic databases (Cogbill 1990). However   this is often not the case for near region part when large-scale topographic product doesn't exist   especially in mountainous areas (Jia   et al.   2009). As gravitational effects become decreased in proportional to the distance from the survey station   near-region terrain correction is more criti-cal than mid and far region correction.

A systematic methodology for performing terrain correction was developed by Hammer (1939). In his method   a template consisting of a series of circles is applied and the center of the circles is placed over the gravity station on the map. Amounts of prisms with increased distance from the center are subsequently made to estimate their individual gravity effect with a formula . By accumulating all the prism's effects   terrain correction is f inished for the gravity station . The practical manual manipulation of Hammer's method is not only complex but also fails to guarantee an accurate value concerning the variation of terrain. Though an improvement was made later by adapting Hammer's formula to be easily implemented by computer (Bott 1959；Kane 1962；Nagy 1966)   the accuracy problem still r emains to be resolved   especially in mountainous areas. Further research has concluded that the Hammer's method could be r efined by using smaller patches or by defining the surface shape more precisely (Campbell 1980；Zhou et al. 1990；Parker 1996). According to China's large-scale gravity exploration spec-ification   the Root Mean Square Error (RMSE) of near region terrain correction (0—20 m) should be within 0. 025 mgal (1 mgal = 10^{-3} cm/s^2) (Sun & Ding 1997). For such a high p recision gravity survey   the near region terrain correction requires a large scale topographic map (1: 2000) or DEM with height accuracy of better than 1 m . As such a large scale topo graphic product often does not exist in mountainous areas   in

practice near region gravity survey usually involves a great deal of manual work. The surveyor usually has to make a large number of measurements using surveying instruments (e. g.   a leveling instrument theodolite or total station) in order to reconstruct the topography (Klingele   1980). Although high precision topographic correction would be expected in this way this classical method is time-consuming and costly which makes it impossible to be widely used in gravity survey work when dealing with a very rugged topography. In fact in practical procedure near r egion gravity survey has long been neglected or simplified in consideration of efficiency and economic reasons which deteriorates the accuracy of gravity survey to some extent (Leanman   1998). Some studies (Yen et al.   1994; Yang et al.   2011) have shown that the amount of terrain correction is closely related to near region topography and near region correction can never be ignored in mountainous areas with high relief. Generally topographic relief plays such an important role that most correction value in these areas is over 20 mgal or even larger while in flat areas the smaller correction value can almost be ignored (Li e t al.   2011). It is highly desirable to develop simple efficient and high precision near region terrain corection method for mountainous areas.

As large part in middle and western China are mountainous areas near region correction must be carefully and efficiently performed in such large areas. It´s apparent that the main challenge for gravity terrain correction is how to rapidly and inexpensively reconstruct high-quality terrain relatively close to the gravity survey station e. g.   within a range of 30 m (Di e t al. 2011). In traditional field surveying the surveyor divides the near region zone into 8 quadrants centering at the gravity s tation and makes measurements of a number of points (e. g.   five points) evenly in each quadrant using total station. Generally it takes a bout 20 minutes to measure nearly 40 points for each s tation and even more time for office work of post processing. In this research we develop a fast near region terrain correction a pproach that significantly outperforms the traditional approach. It can automatically generate about 6000 three-dimensional points within two minutes (including data acquisition and data processing). This new approach is based on panoramic stereo v ision and photogrammetry techniques. As the attainable accuracy of this method is largely determined by the measurement accuracy a theoretical analysis of the measurement accuracy at different distances is performed and a suitable set of geometric configurations of stereo vision is chosen. Accordingly a fast and low-cost topographic mapping system is designed and developed including hardware and software for data acquisition and processing. In the field tests with various terrain circumstances our method has proved its efficiency accuracy and r obustness compared to traditional field surveying approach.

It is worth to note that panoramic imaging technology has been widely used in "street view" image acquisition for web mapping services such as Google Earth; stereo panoramic images have been used in navigation and mapping on the Mars exploration rover mission (Di & Li 2007; Di & Ge 2011). The contribution of this paper is to introduce the stereo panoramic v ision technology into the field of gravity terrain correction and to design and develop a fast and low-cost topographic mapping sys-

tem for practical application in near-region gravity terrain correction.

2 HARDWARE DESIGN AND THEORETICAL ACCURACY ANALYSIS

2.1 Hardware design of the topographic mapping system

The measurement accuracy of a stereo mapping system is largely determined by it´s hardware design. As is shown in Fig. 1 the hardware of the system includes a pair of CCD cameras for stereo image acquisition a rotary stage to rotate the cameras and a tripod for holding the imaging system. The stereo cameras are mounted on the two ends of a camera bar which is fixed to the two-degree-of-freedom rotary stage. The rotary stage can rotate ±180° horizontally and ±36° vertically so that the system acquires panoramic stereo images around a gravity station. A laptop computer is used to control the cameras and the rotary stage.

Fig. 1   Hardware of the topographic correction system

The geometric configuration parameters of the hardware components are listed in Table 1.

Table 1   Geometric parameters of the stereo camera system

Stereo camera	Camera type	MV-VE141SC/SM
	Stereo base	50 cm
	Focal length	12 mm
	Image dimension	1392 × 1040 pixels
	Pixel size	6. 45 μm × 6. 45 μm
Rotary stage	Vertical range	−36°—36°
	Horizontal range	−180°—180°
	Accuracy	0. 0129°
Laptop computer	CPU	Intel core i3 2. 13 GHz

These hardware components are determined by the following theoretical analysis of measurement accuracy. The idea is to select the low-cost but reliable components that satisfy the accuracy requirement of near-region gravity terrain correction rather than to select high-end components that achieve the highest accuracy.

2.2 Theoretical analysis of measurement accuracy

In order to perform near region terrain correction it is i

mportant to analyze the attainable measurement accuracy of the stereo camera system. Actually, the selection of camera and the setting of the baseline (Table 1) are based on theoretical measurement accuracy analysis. In our hardware system, the principal rays of the two cameras are parallel to each other and perpendicular to the baseline as depicted in Fig. 2.
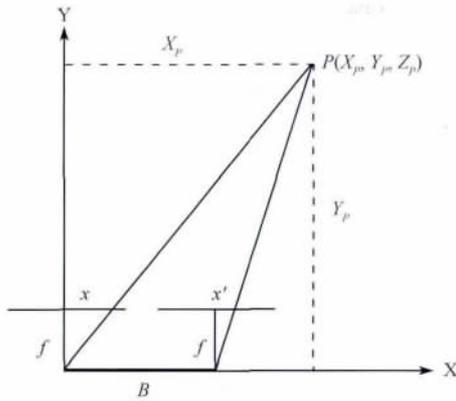

Fig. 2   "Normal case" stereo configuration (Di & Li, 2007)

For such a "normal case" stereo configuration, the three dimensional coordinates of object point $P(X_p, Y_p, Z_p)$ can be calculated using the following parallax equations

$$\begin{cases} Y_p = \dfrac{B}{p}f \\ X_p = \dfrac{B}{p}x = \dfrac{Y_p}{f}x \\ Z_p = \dfrac{B}{p}y = \dfrac{Y_p}{f}y \end{cases} \quad (1)$$

where f is the focal length of the camera, B is the length of stereo baseline, p is the stereo parallax of the corresponding points which is calculated as $p = x - x'$, here taking x and x' to be the horizontal position of the points in the left and right image, respectively (Fig. 2).

Based on Eq. (1), the attainable accuracy is obtained from theoretical derivation. Through error propagation, the accuracies (standard errors σ_Y, σ_X, σ_Z) are represented as (Di & Li, 2007; Di & Peng, 2011)

$$\begin{cases} \sigma_Y = \dfrac{Y_p^2}{Bf}\sigma_p \\ \sigma_X = \sqrt{\left(\dfrac{Y_p^2}{Bf}\right)^2\left(\dfrac{x}{f}\right)^2\sigma_p^2 + \left(\dfrac{Y_p}{f}\right)^2\sigma_x^2} \\ \sigma_Z = \sqrt{\left(\dfrac{Y_p^2}{Bf}\right)^2\left(\dfrac{y}{f}\right)^2\sigma_p^2 + \left(\dfrac{Y_p}{f}\right)^2\sigma_y^2} \end{cases} \quad (2)$$

where σ_p is the parallax measurement error, σ_x and σ_y are the image measurement errors in X and Y directions in image space. From Eq. (2), we can easily come to a qualitative conclusion that the measurement error reduces when the focal length and the baseline length increase. This suggests that larger focal length and baseline are preferable if possible. It is obvious that the range error σ_Y is proportional to the square of the range Y_p and that the measurement errors in X and Z directions are dependent on not only the range, but also the position of the object in the image. At a given range, the minimum error of X direction lies on the vertical line passing through the image

center (where $x = 0$), while the maximum errors of X direction lie on the left and right margins of the image. Similarly, at a given range, the minimum error of Z lies on the horizontal line passing through the image center (where $y = 0$), while the maximum errors of Z direction lie on the top and bottom margins of the image.
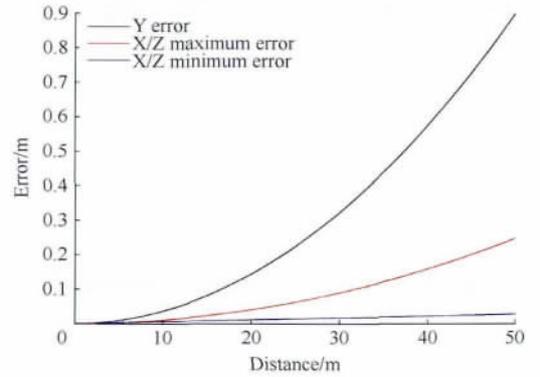

Fig. 3   Theoretical measurement accuracy at different ranges

The parallax measurement accuracy is determined by the accuracy of image matching. According to a theoretical analysis, pixel-level image matching (correlation) has an accuracy of about 1/3 pixel (Zhang & Zhang, 1997), while least-squares matching has an even higher accuracy. Given $\sigma_p = 1/3$ pixel, $\sigma_x = \sigma_y = 1$ pixel, and the parameters of the cameras, the standard errors at different ranges are calculated by Eq. (2) and shown in Fig. 3.

As is clearly seen in Fig. 3, the measurement error in the range direction is always larger than that in the other two directions, and measurement accuracies in three directions are all better than 1 m within 50 m, which satisfies the requirements of near region terrain correction.

2.3   Calibration of stereo cameras

It is critical to calibrate the cameras in order to achieve the theoretical mapping accuracy. The task of camera calibration is to determine the interior orientation parameters (focal length, position of principal point) and optical distortion parameters of each camera, and the relative orientation parameters between the two cameras.

Camera calibration is performed at a calibration range where hundreds of precisely measured control points are evenly distributed in a three dimensional space (Fig. 4). The internal camera model used in this calibration is very similar to that used by Heikkila and Silven (1997), which can generally deal with camera distortion very efficiently. To reduce the time of manual measurement of the control points in the images, we developed a semi-automatic method for control point measurement. We only need to manually measure several control points (green crosses in Fig. 4), then the rest of control points (red crosses in Fig. 4) are extracted automatically by least squares template matching. As we can see, most control points in the image are extracted successfully, which are sufficient for camera calibration. Based on these control points, interior orientation parameters, optical distortion parameters, and exterior orientation

parameters are determined through a least squares solution of space resection with collinearity equations (Feng 2002). The accuracy of camera calibration is evaluated by the root mean square residual on the control points which turned out to be within 0.2 pixel for both the left and right camera.

Fig.4   Camera calibration range

In order to calibrate the relative orientation and translation of the two cameras images of the three dimensional calibration range are captured simultaneously by the stereo cameras. Multiple pairs of images are used to improve accuracy and robustness in the calibration. After calibration we get the left camera's position vector T_{left} and orientation matrix R_{left} right camera's position vector T_{right} and orientation matrix R_{right} which are defined in the calibration range coordinate system. Taking the left camera as the reference camera the relative relation of these two cameras can be represented as

$$\begin{cases} R_{l/r} = R_{left}^{-1} \cdot R_{right} \\ T_{l/r} = R_{left}^{-1} \cdot (T_{right} - T_{left}) \end{cases} \quad (3)$$

where $R_{l/r}$ and $T_{l/r}$ are the right camera's orientation and translation relative to the left camera.

To validate the effectiveness of our model of calibration we performed many outdoor experiments. By comparing our measurements with ground check points measured by differential GPS the three dimensional measurement accuracy is consistent with the theoretical accuracy. The height accuracy is within 0.5 m using the calibrated parameters meeting the accuracy requirement for near-region terrain correction.

2.4   Calibration of the rotary stage

The acquisition of panoramic images around the survey station is realized by rotating the rotary stage. Thus the exterior orientation parameters of the images are determined by the rotary stage's horizontal (azimuth) and vertical (tilt) angles. Ideally after the rotary stage is leveled the cameras move on a horizontal plane when the rotary stage rotates horizontally and move on two vertical planes when the rotary stage rotates vertically. In reality due to the installation limitations and errors there are unavoidable offsets for the rotating axes and the rotating centers. In order to get accurate exterior orientation parameters the actual position and orientation of both vertical and horizontal rotating axes should be determined.

We establish the rotary stage coordinate system as Fig.5

illustrates: the origin is set to be the center of the baseline of the stereo cameras; the X and Z axis lie on the horizontal base plane and the Y axis lies vertically; L_V is the vertical rotating axis and L_H is the horizontal rotating axis. In order to calibrate these two rotating axes' offsets and the origin offset the rotary stage is set to be within the three dimensional calibration range. A series of images are taken at different horizontal and vertical angles: first the rotary stage rotates $-35°$ vertically and then rotates $-360°$ horizontally at $5°$ intervals and stereo images are acquired at these stops; second the rotary stage rotates vertically by an increment of $5°$ and the process of horizontal rotation and image acquisition repeats as in the first step; the vertical rotation finishes until the vertical angle reaches $35°$. Through space resection with collinearity equations a series of camera's discrete orientation can be determined and the camera's circular trajectory can be fitted through a least squares solution. As a rotating axis is orthogonal to the corresponding circular trajectory its actual location and orientation can be determined which are as $A_P^H(p_1\ v_1)$ and $A_P^V(p_2\ v_2)$ for horizontal and vertical axis respectively. Here p_1 and v_1 represent the position and orientation of the vertical rotation axis while p_2 and v_2 represent the position and orientation of the horizontal rotation axis.
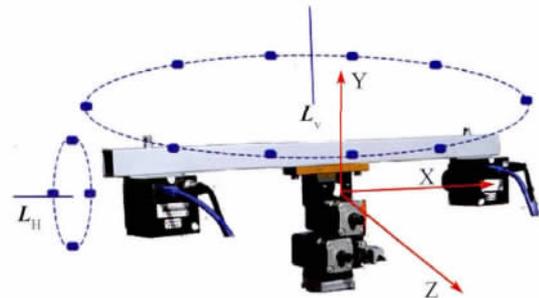

Fig.5   Rotary stage coordinate system

2.5   Calculation of exterior camera parameters

When the rotary stage's horizontal and vertical angels are set to 0 the initial state of stereo cameras in the rotary stage coordinate system can be calculated as

$$\begin{cases} R_{L0} = R(v_2) \cdot R(v_1) \cdot R(0\ 0\ 0) \\ T_{L0} = R_{L0} \cdot ((-L/2\ 0\ 0)^T - p_1) \\ R_{R0} = R(v_2) \cdot R(v_1) \cdot R_{r/l} \cdot R(0\ 0\ 0) \\ T_{Ro} = R_{R0} \cdot ((L/2\ 0\ 0)^T - p_2) \end{cases} \quad (4)$$

where L is the baseline length of stereo cameras R_{L0} and T_{L0} denote the left camera's initial exterior parameters (rotation matrix and translation vector) R_{R0} and T_{Ro} denote the right camera's initial exterior parameters.

Given the rotary stage's horizontal angle θ and vertical angle ϕ the camera's exterior parameters R and T can be accurately calculated as

$$\begin{cases} R = R(\phi\ 0\ 0) \cdot R(0\ \theta\ 0) \cdot R_0 \\ T = R \cdot T_0 \end{cases} \quad (5)$$

where R_0 and T_0 are camera's initial state and are substituted by R_{L0} T_{L0} and R_{R0} T_{Ro} to calculate the left and right camera's exterior orientation parameters.

3　THREE-DIMENSIONAL TERRAIN RECO-N STRUCTION AND NEAR REGION TERRAIN CORRECTION

The software system can generate near region terrain correction value automatically by the means of batch processing based on panoramic stereo images captured around the survey station　which largely reduces manual labor. There are mainly two steps in the process：（1）three-dimensional point cloud generation and filtering in order to produce high quality DEM；（2）topographic correction based on the DEM. The flowchart of this process is illustrated in Fig. 6.
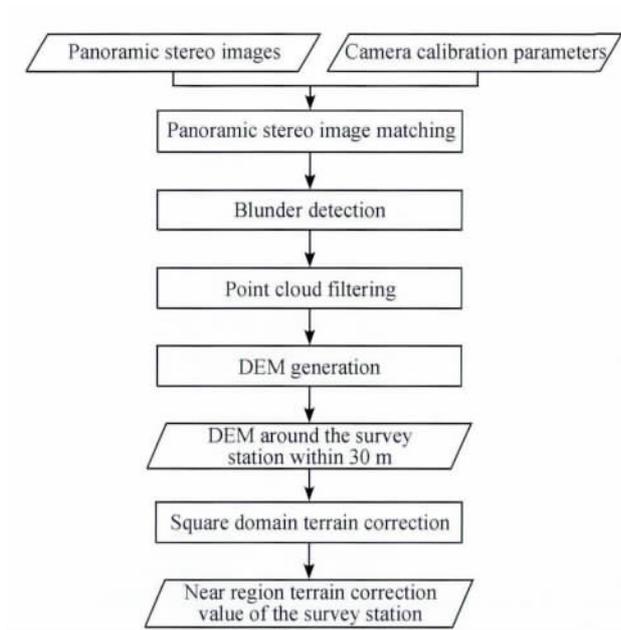

Fig. 6　Flowchart of three-dimensional terrain reconstruction and gravity terrain correction

3. 1　Point cloud generation and blunder detection

First　radiometric enhancement is conducted by Gaussian filter to remove image noises. Then　by applying Förstner operator（Förstner & Güelch　1987）with proper threshold mass feature points are detected in the images. To make the detected points well distributed in the whole image and adaptive to local terrain conditions　the image is divided into tens of grids and in each grid certain amount of points are detected by adjusting the operator threshold within the grid. Afterwards　stereo image matching is performed by using normalized correlation coefficients method on the detected feature points from the stereo images. Least squares matching method is further applied to achieve sub-pixel matching precision. Constraints of local disparity consistency and epipolar geometry are imposed to improve the reliability and efficiency of the stereo matching. Finally　three-dimensional positions of the matched points are calculated using space intersection with collinearity equations. Generally　more than 6000 three-dimensional points are generated this way at one station using 12 pairs of stereo images.

It is usually unavoidable that blunder exists in three dimensional point cloud. A blunder detection algorithm（Li & Zhu　2000）is adopted. The main idea of the algorithm is as the following：（1）for each point P　a window with fixed size centered at P is defined and the median height value is found within the window；（2）if the difference between the height and the median is above a certain threshold　P is detected as a blunder and removed. The above threshold is determined automatically by a statistical analysis：（1）for each window the difference of each point's height with the mean height value of the rest of the points within the window is calculated；（2）the threshold is three times of the root mean square difference.

3. 2　Point cloud filtering and terrain reconstruction

As above-earth points are also mixed in the point cloud they need to be removed in order to reconstruct bare-earth terrain. A slope-based morphological filtering algorithm（Vosselman　2000）is applied for this purpose. Point cloud is filtered by defining such a slope-based core function represented as：

$$\begin{cases} \boldsymbol{\Omega} = \{ p_i \in \boldsymbol{A} \mid \forall p_j \in \boldsymbol{A}: |h_{p_i} - h_{p_j}| \leqslant \Delta h_{\max}(d(p_i\ p_j)) \} \\ \Delta h_{\max} = \theta_{\text{slope}} \times d \end{cases} \quad (6)$$

where d is the horizontal distance between the two points　θ_{slope} is the slope threshold　$\Delta h_{\max}$ is the maximum height difference　$\boldsymbol{\Omega}$ is the filtered point cloud. A point is accepted only when the height difference between the point and other points in the neigh-borhood is not above $\Delta h_{\max}$. By traversing the point cloud　all the above-earth points are rejected.

However　it is difficult to define a uniform slope threshold as the terrain varies. An adaptive point cloud filtering algorithm（Zhou　2004）is applied to tackle the problem. The algorithm main-ly includes the following steps：（1）by dividing the point cloud u-sing sparse grid　an adaptive slope threshold for each grid is deter-mined through plane fitting using the three dimensional points within the sparse grid cell；（2）for each sparse grid　filter out the points which don't obey the rule described by Eq.（6）；（3）by dividing the point cloud using dense grid　a similar procedure of（1）and（2）is applied；（4）by reducing the sparse grid width by a factor of 2　the iteration continues until the sparse grid width equals the dense grid width. In our experiment　the widths of the sparse and dense grids are set to be 5 m　0. 5 m respectively.

As the three dimensional points are defined in the rotary stage's coordinated system（leveled through the tripod）　in order to obtain the three dimensional points' absolute height in geodetic coordinate system　the gravity station's absolute height and the rotary stage's relative height above the earth are needed. For each survey station　the absolute geodetic height can be o btained by GPS while the relative height is manually measured by a steel tape. It is worth to note that absolute azimuthal correction is not needed for the purpose of topographic correction.

Finally　DEM can be reconstructed from filtered three d imensional point clouds by kriging interpolation method.

3. 3　Topographic correction

As the automatically generated DEM is stored as square grid data　topographic correction value is conveniently calculated with

square domain method（Jiang 1988；Shen 1993；Feng 2007）. Fig. 7 shows how this terrain correction method is performed around the survey station.
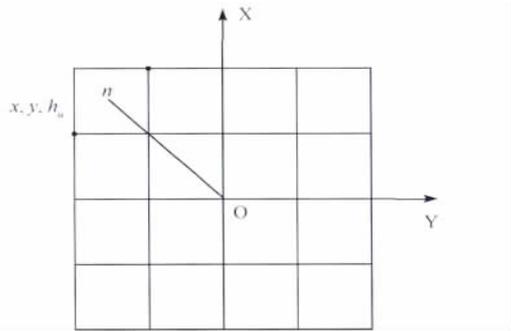

Fig. 7   Square domain method for topographic correction

In Fig. 7 O is the survey station and n is the center of the grid cell with the grid size of 1 m（such a resolution meets the requirement of near-region terrain gravity correction）. Then the terrain correction value of that grid is calculated as（Jiang 1988）

$$\Delta g_n = f\sigma \iint \left(1 - \frac{\sqrt{x^2 + y^2}}{\sqrt{x^2 + y^2 + h_n^2}}\right)\frac{1}{(x^2 + y^2)^{1/2}}dxdy \quad (7)$$

where $f = 6.67 \times 10^{-8}$ is the gravitational constant σ is density of rocks constructing the terrain x and y are the horizontal and vertical coordinate in the survey station coordinate system h_n is the

grid cell's absolute height.

By summing up all grid cells' terrain effects the gravity correction value of the survey station is finally calculated as

$$\Delta g = \sum \Delta g_n . \quad (8)$$

4   EXPERIMENTAL RESULTS

Experiments and field tests have been performed to verify the developed system. In the field test in the area of Ming Tombs in Beijing suburb panoramic stereo images were collected at 15 stations with various terrain circumstances. Here we report the results of two typical gravity stations. The terrain of station A is relatively flat; station B has larger terrain relief and slopes. Panoramic images at the two stations are shown in Fig. 8 and Fig. 9 respectively. DEMs of the two stations（60 m × 60 m）are automatically generated with a required 1 m resolution. Fig. 10 shows the DEM of station A before and after point cloud filtering. Fig. 11 shows the DEM of station B before and after point cloud filtering. Here X Y and Z are horizontal and vertical coordinate in the survey station coordinate system. As we can clearly see from Fig. 8 the environment surrounding the gravity station is covered with a lot of grass which poses a real challenge for image matching and DEM generation. As a result many blunders appear randomly in the generated DEM without point cloud filtering. From the final DEMs it can be seen that point cloud filtering can effectively remove blunders and above-earth points.
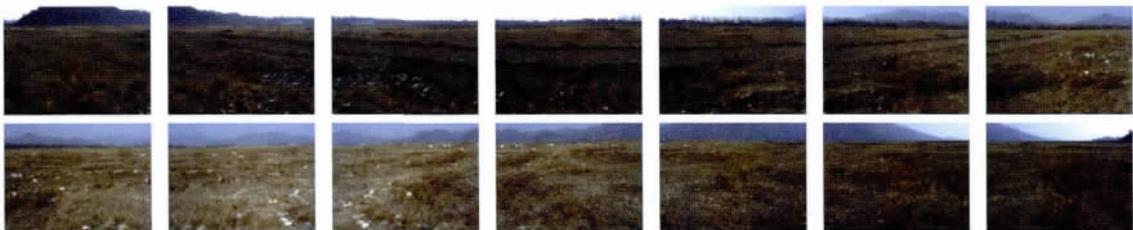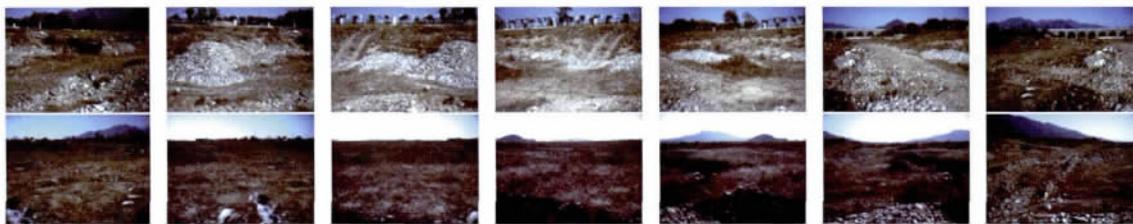

Fig.8   Panoramic image sequences of station A
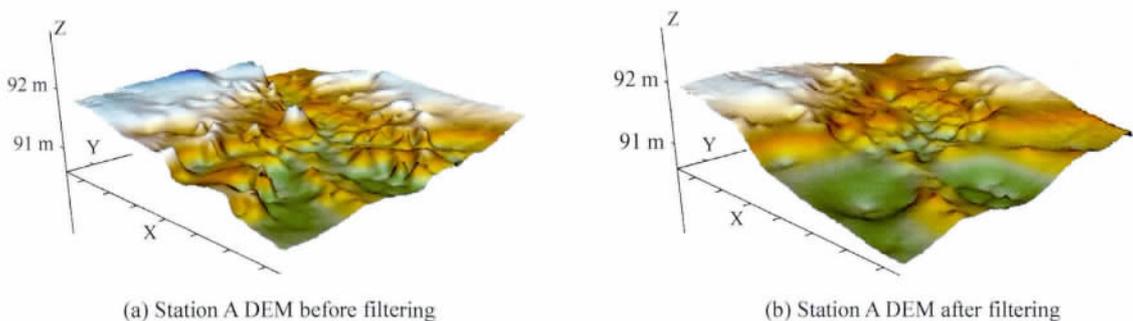

Fig.9   Panoramic image sequences of station B

(a) Station A DEM before filtering

(b) Station A DEM after filtering

Fig.10   Station A DEM

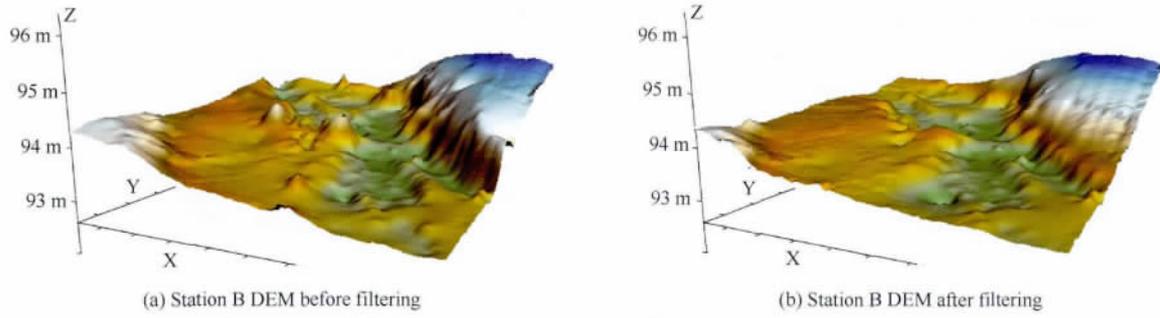(a) Station B DEM before filtering　　　(b) Station B DEM after filtering

Fig. 11　Station B DEM

In order to evaluate the accuracy of terrain reconstruction and correction 1:500 large-scale maps and high quality DEMs of the field test area were produced through a large-scale filed survey using differential GPS and total station with high density of sampling points at least one point per square meter. The densely measured ground points DEM and derived topographic correction values are used as ground truths (references) in the following comparisons.

In our experiments we evaluate the DEM accuracy using a series of check points (60 points for A and 89 points for B) evenly distributed in the 60 m × 60 m square areas by comparing the heights at given horizontal positions with their actual height values. Fig. 12 and Fig. 13 are the height error histograms of the two DEMs. The RMSEs are 0. 46 m and 0. 84 m respectively which satisfy the required accuracy of 1 m.
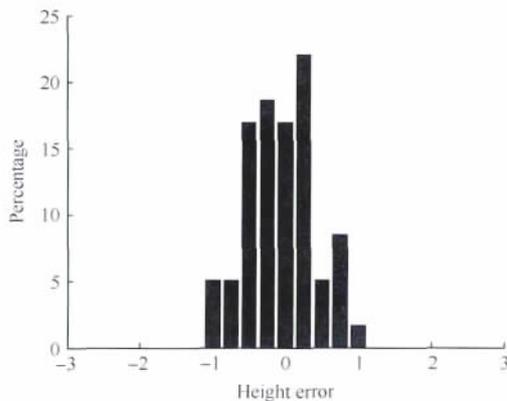

Fig.12　Station A DEM error histogram

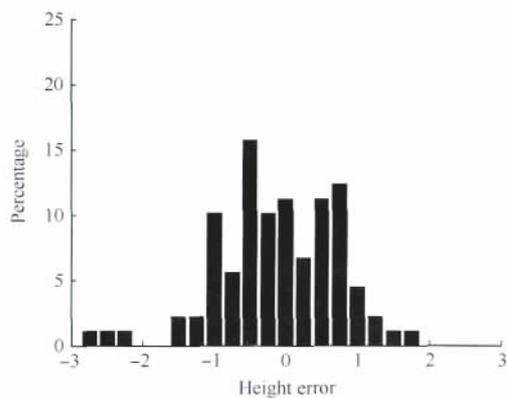
Fig.13　Station B DEM error histogram

It can be seen from the figures that the error distributions generally satisfy normal distribution. Meanwhile the height a ccuracy of the flatter terrain is better than that of the terrain with larger slopes. This is due to two reasons: occlusions are likely to exist in the images of the terrain with larger slopes which may decrease the final accuracy; horizontal accuracy has a larger effect on height accuracy of the DEM in larger slopes. O verall the actual mapping accuracy is generally consistent with the theoretical accuracy.

Having obtained the DEM for each station the topographic correction values from our new method are calculated and c ompared with the reference values and the values calculated from the traditional method of total-station based field surveying. The reference topographic correction values are derived from high qualities DEMs mentioned above (derived from very dense ground points measured by differential GPS and total station) while the correction values of the traditional method are calculated from sparse ground points (40 points in each gravity station) measured by total station. Table 2 shows the comparison results.

Table 2　Topographic correction accuracy comparison

Station No.	Reference/ mgal	Traditional method/ mgal	New method/ mgal	Error for traditional method/mgal	Error for new method/ mgal
1	0.04353	0.05775	0.04541	0.01422	0.00188
2	0.01705	0.03091	0.0157	0.01386	−0.00135
3	0.00958	0.00005	0.01200	−0.00953	0.00242
4	0.00612	0.00277	0.0087	−0.00335	0.00258
RMSE/ mgal				0.01114	0.00211

From Table 2 above the accuracy of our new method is much higher than that of the traditional field surveying method. In fact the RMSE gets largely decreased from 0. 01114 mgal to 0. 00211 mgal by using our new method compared to the traditional methods. Since our mapping system automatically collects much denser three-dimensional points of the terrain than traditional field surveying thus the overall accuracy of the DEM for topographic correction is generally higher. This is particularly significant for mountainous areas where the traditional method would need to measure more points in order to achieve satisfactory accuracy.

Referring to efficiency for each station the panoramic image (12 stereo pairs) acquisition time is about 60 s and the a

utomatic DEM generation time is about 35 s. For most of the test stations the terrain correction process is fully automatic without human intervention. For some stations where there are dense trees some manual operation is necessary which may take several minutes. Overall in addition to accuracy improvement this is a significant improvement in efficiency over the traditional field surveying method.

5 CONCLUSIONS

In this paper we presented a fast near-region gravity terrain correction approach based on panoramic vision. As a complete system the hardware design system calibration theoretical accuracy and the automated DEM generation techniques are described. The experimental results demonstrate that the developed system significantly outperforms the traditional field surveying method in efficiency and accuracy. The aim of the s ystem is to reach the required accuracy with low-cost and reliable hardware components along with dedicated software rather than to achieve highest accuracy using high-end hardware components. The software system will be further enhanced in the future. More field tests will be performed to validate this new system so that it can be applied in practical applications in topographic correction for regional gravity survey.

REFERENCES

Bott M H P. 1959. The use of electronic digital computors for the evaluation of gravimetric terrain corrections. Geophysical Prospecting 7 (1): 45 –54   DOI: 10.1111/j.1365 –2478.1959.tb01452.x

Campbell D L. 1980. Gravity terrain corrections for stations on a uniform slope—a power law approximation. Geophysics 45(1): 109 –112   DOI: 10.1190/1.1441035

Cogbill (Allen) H. 1990. Gravity terrain corrections calculated using digital elevation models. Geophysics 55(1): 102 –106   DOI: 10.1190/1.1442762

Di K C and Ge Z J. 2011. A brief review of Spirit's six years of Mars roving and scientific discoveries. Journal of Remote Sensing 15(4): 651 –658

Di K C and Li R X. 2007. Topographic mapping capability analysis of mars exploration rover 2003 mission imagery // Proceedings of 5th International Symposium on Mobile Mapping Technology (MMT 2007). Padua Italy: 28 –31

Di K C and Peng M. 2011. Wide baseline mapping for mars rovers. Photogrammetric Engineering and Remote Sensing 77(6): 609 –618

Di K C Wu K Liu Z Q Wan W H Di Z Z and Li G. 2011. A fast topographic mapping system based on panoramic vision for near region terrain correction in region gravity survey // Proceedings of the 32nd Asian Conference on Remote Sensing. Taipei China

Fan X F. 2007. On fast calculation for the near region terrain correction of the regional gravity survey. Chinese Journal of Engineering Geophysics 4(6): 560 –562

Feng W H. 2002. Close-range camera calibration // Wang J L ed. Close-range Photogrammetry. Wuhan: Wuhan University Press: 185 –215

Feng Z H. 2007. A tentative discussion on the median region gravity terrain correction method in regional gravity survey. Geophysical and

Geochemical Exploration 31(5): 455 –459

Förstner W and Güelch E. 1987. A Fast operator for detection and precise location of distinct points corners and centers of circular features // ISPRS Intercommission Workshop on Fast Processing of Photogrammetric Data. Interlaken Switzerland: 281 –305

Hammer S. 1939. Terrain corrections for gravimeter stations. Geophysics 4(3): 184 –194   DOI: 10.1190/1.1440495

Heikkila J and Silven O. 1997. A four-step camera calibration procedure with implicit image correction // Proceedings of the IEEE Computer Society Conference on Computer Vision and Pattern Recognition. San Juan Puerto Rico: IEEE 1106 –1112   DOI: 10.1109/CVPR.1997.609468

Jia R Z Davis L and Groom R W. 2009. New approaches to topographic gravity corrections // Proceedings of the 22th EEGS Symposium on the Application of Geophysics to Engineering and Environmental Problems. Texas: Curran Associates

Jiang Y L. 1988. Research on near region gravity corrction method of square domain. Geology and Exploration 5: 37 –40

Kane M F. 1962. A comprehensive system of terrain corrections using a digital computer. Geophysics 27(4): 455 –462   DOI: 10.1190/1.1439044

Klingele E. 1980. A new method for near-topographic correction in gravity surveys. Pure and Applied Geophysics 119(2): 373 –379   DOI: 10.1007/BF00877772

Leanman D E. 1998. The gravity terrain correction-practical considerations. Exploration Geophysics 29(4): 467 –471   DOI: 10.1071/EG998467

Li Z H Li Q and Lin X. 2011. Research on the terrain correction models in gravity survey. Engineering of Surveying and Mapping 20(2): 24 –26

Li Z L and Zhu Q. 2000. Digital Terrain Model. Wuhan : Wuhan Technical University of Surveying and Mapping Press: 93 –101

Nagy D. 1966. The prism method for terrain corrections using digital computers. Pure and Applied Geophysics 63(1): 31 –39   DOI: 10.1007/BF00875156

Parker R L. 1996. Improved Fourier terrain correction Part II. Geophysics 61(2): 365 –372   DOI: 10.1190/1.1443965

Shen Z M. 1993. Programming of near-region terrain correction for high precision gravity survey. Computing Techniques for Geographical and Geochemical Exploration 15(2): 175 –177

Sun W K and Ding P F. 1997. DZ/T 0171 –1997 Large scale gravity exploration specification. Ministry of Geology and Mineral Resources. pp. 5 –6

Vosselman G. 2000. Slope based filtering of laser altimetry data. International Archives of Photogrammetry and Remote Sensing Amsterdam XXXIII: 935 –942

Yang Y B Han G M and Liang M. 2011. Gravity near zone terrain correction precision discussion. Computing Techniques for Geophysical and Geochemical Exploration 33(1): 92 –96

Yen H Y Yeh Y H and Chen C H. 1994. Gravity terrain corrections of Taiwan. Terrestrial Atmospheric and Oceanic Sciences 5(1): 1 –10

Zhang Z X and Zhang J Q. 1997. Digital Photogrammetry. Wuhan: Wuhan Technical University of Surveying and Mapping: 171 –172

Zhou F C. 2004. An Adaptive Point Cloud Filtering Algorithm for DEM Generation from Airborne Lidar Data. Taiwan: Cheng Kung University: 27 –42

Zhou X Zhong B and Li X. 1990. Gravimetric terrain corrections by triangular-element method. Geophysics 55(2): 232 –238   DOI: 10.1190/1.1442831

1   1   1   1   2   2

1.   100101;

2.   100085

:   、   。

。   3

。

。

。

`   (±180°   ±

36°)

。

50 m   3   1 m

。

`            `

360°   、

30 m   ;

Kringing   DEM

3   ;

。

5 min

。

:

: TP79   : A

:   . 2013.   .   17(4):

759 −767

Di K C Wu K Liu Z Q Wan W H Di Z Z and Li G. 2013. Fast near-region gravity terrain correction approach based on panoramic stereo vision. Journal of Remote Sensing 17(4): 759 −767   DOI: 10. 11834/jrs. 20132218